PROJECT ECHO

A Horn-Reflector Antenna for Space Communication

By A. B. CRAWFORD, D. C. HOGG and L. E. HUNT

(Manuscript received April 7, 1961)

This paper describes the mechanical features of the horn-reflector antenna used for receiving signals reflected from the Project Echo balloon satellite and presents in some detail the electrical characteristics (radiation patterns and gain) measured at a frequency of 2390 mc. Theoretically derived characteristics which agree very well with the measurements are also presented; details of the calculations are given in the appendices.

I. INTRODUCTION

The horn-reflector type of antenna was originated at Bell Telephone Laboratories, Holmdel, New Jersey, in the early 1940's[1] and is now in extensive use in the Bell System's transcontinental microwave relay network.[2] It is a combination of a square electromagnetic horn and a reflector that is a sector of a paraboloid of revolution, as illustrated in Fig. 1. The apex of the horn coincides with the focus of the paraboloid. Since the antenna design is based on geometrical optics and has no frequency-sensitive elements, it is extremely broadband; it is not polarization-sensitive and can be used in any linear or circular polarization. The antenna is essentially an offset paraboloidal antenna, so that very little of the energy incident on the reflector is reflected back into the feed to produce an impedance mismatch. Due to the shielding effect of the horn, the far side and back lobes are very small.

These features, together with high aperture efficiency, make the horn-reflector attractive for use in satellite communication systems. In particular, the low side and back lobes insure that when the antenna beam is pointed to the sky very little noise power is received from the ground;* the antenna is thus a low-noise transducer which permits exploitation

* A discussion of the noise properties of antennas is given in Ref. 3.

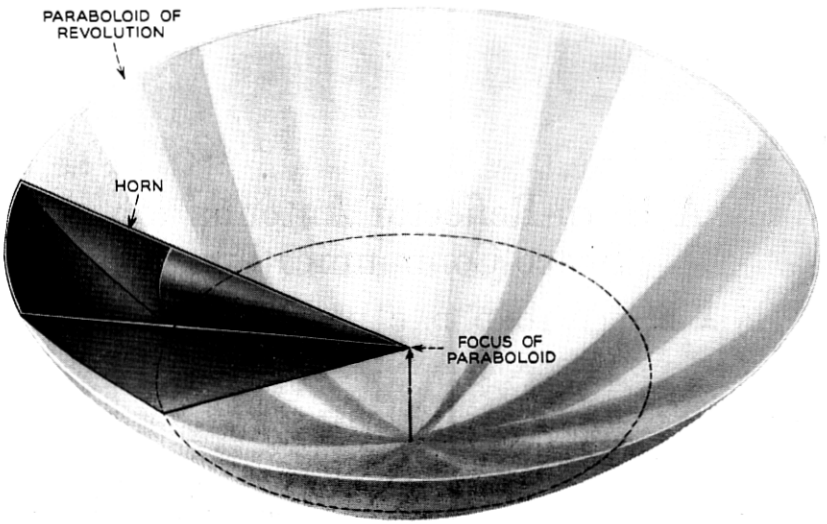

Fig. 1 — Sketch showing relationship of horn-reflector antenna to a paraboloid of revolution.

of the low-noise features of the maser amplifier. An effective noise temperature of about 2°K has been measured for the horn-reflector type of antenna.[4]

II. MECHANICAL DESCRIPTION OF THE ANTENNA

Fig. 2 is a photograph of the horn-reflector antenna erected on the Crawford Hill site of the Holmdel Laboratory and used in the Project Echo experiment.* To permit the antenna beam to be directed to any part of the sky, the antenna is mounted with the axis of the horn horizontal. Rotation about this axis affords tracking in elevation while the entire assembly is rotated about a vertical axis for tracking in azimuth. The antenna is about 50 feet in length, the radiating aperture is approximately 20 by 20 feet, and the weight is about 18 tons. The structure was designed to survive winds of 100 miles per hour.

The elevation structure, both horn and reflector, is constructed of aluminum. The elevation wheel, 30 feet in diameter, supports all radial loads and rotates on rollers mounted on the base frame. All axial or thrust loads are taken by a large ball bearing at the apex end of the

* Although this antenna was designed and constructed by the Bell System as part of its research and development program, it was operated in connection with Project Echo under Contract NASW-110 for the National Aeronautics and Space Administration.

horn. The horn proper continues through this bearing into the equipment cab. Here is located a tapered transition section from square to round waveguide, a rotating joint, and waveguide take-offs which provide for the simultaneous reception of either two orthogonal linearly polarized signals or two circularly polarized signals of opposite sense. The ability to locate the receiver equipment at the apex of the horn, thus eliminating the loss and noise contribution of a connecting line, is an important feature of this antenna.

The triangular base frame is constructed of structural steel shapes. It rotates on wheels about a center pintle ball bearing on a track 30 feet in diameter. The track consists of stress-relieved, planed steel plates which were individually adjusted to produce a track flat to about $\frac{1}{64}$ inch. The faces of the wheels are cone-shaped to minimize sliding friction. A tangential force of about 100 pounds is sufficient to start the antenna in motion.

The horn flares at an angle of 28°. As can be seen in Fig. 1, the antenna is generated by swinging the side projection through this angle. Thus the two sides of the horn are flat surfaces, while the front and back surfaces are sections of cones. There are several advantages to this type of construction: right-angle sections can be used for the corners of the horn; the reflector can be constructed of identical longitudinal sections;

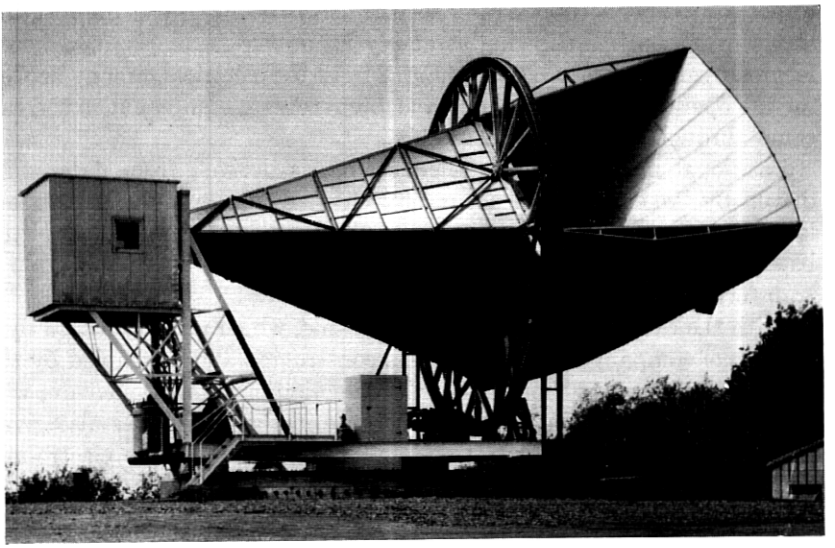

Fig. 2 — Horn-reflector antenna used in Project Echo experiment.

the intersections of the front and back conical surfaces with the paraboloid of revolution are circles in planes perpendicular to the axis of the paraboloid, thus providing accurate and readily available references for use in constructing the reflector. Nine accurately fabricated parabolic ribs were used for the reflector, one end of each being fastened to a curved (arc of a circle) beam at the wheel while the other end was fixed on a circle scribed on a temporary horizontal work table. The ribs were tied together by cross bracing and by a large triangular crossbeam, which in turn was tied by columns to the vertical wheel. The aluminum sheets that make up the reflecting surface were then fastened to the ribs; these have curved stiffeners to produce the small curvature required in the plane perpendicular to the ribs. It is believed that the reflector surface is accurately paraboloidal to $\pm\frac{1}{32}$ inch.

The antenna is driven in azimuth and elevation by 10 H.P. direct-current servo gear-motors.* Power is transmitted by sprockets (with teeth specially cut for rack operation) to roller chains which are fastened to the vertical wheel and to the plates forming the horizontal track. The roller chain proved to be a satisfactory substitute for a large bull gear; by the use of a radial arm and dial indicator, the rollers of the chains were adjusted to lie on 30-foot-diameter circles to an accuracy of about 0.005 inch. The maximum speed of rotation in both azimuth and elevation is 5° per second; the maximum acceleration for both axes is 5° per second per second. Power for the drives is brought to the rotating structure through a slip-ring assembly inside the small plywood house located over the center bearing (Fig. 2). All the electrical circuits needed for the operation of the antenna and the receiving equipment in the cab come through the slip-ring assembly.

Positional information for the antenna is derived from data units driven by large (48-inch) accurately cut and accurately aligned gears located on the bearings at the apex of the horn and at the center of the base frame. The data units contain synchro transmitters and control transformers operated in a two-speed, 1:1 and 36:1, system.

With the exception of the steel base frame, which was fabricated by a local steel company, the antenna was constructed and assembled by the Holmdel Laboratory shops under the direction of H. W. Anderson, who also collaborated in the design. Assistance in the design was also given by R. O'Regan, S. A. Darby and several members of the electro-mechanical development group at the Whippany Laboratory. The latter group also was instrumental in procuring special equipment such as data units, gears, and slip-ring assembly.

* This is more power than required, particularly for the elevation drive, but these motor and control packages were standard items and were readily available.

The antenna has performed well electrically and mechanically during the Project Echo experiment. It was subjected to winds of 80 mph during Hurricane Donna, September 12, 1960, without damage. It has been customary to disengage the azimuth sprocket drive when the antenna is not in use, thus permitting the structure to "weathervane" and seek a position of minimum wind resistance.

III. THEORETICAL DISCUSSION

The manner in which the spherical wave diverges from the apex of the horn is shown schematically in Fig. 3(a). This wave, for the greater

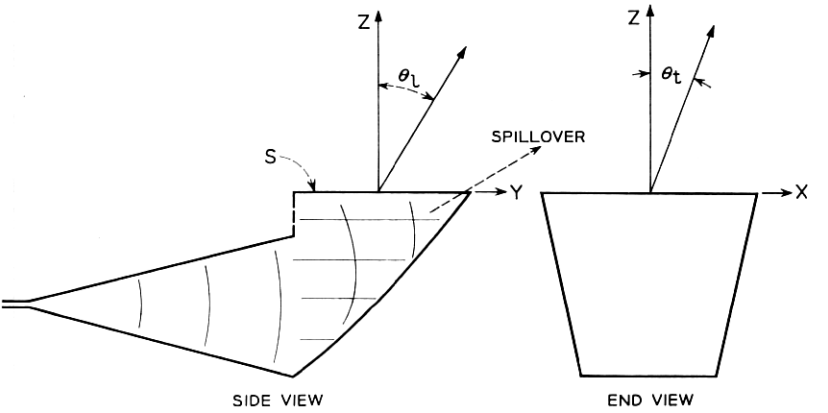

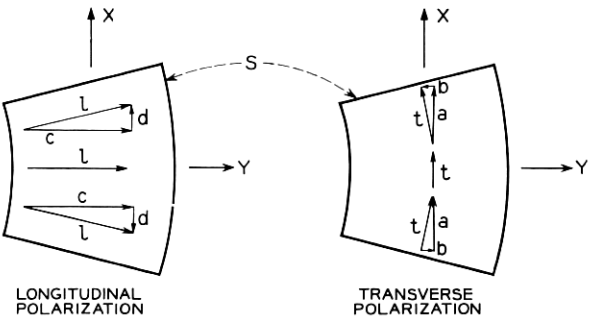

Fig. 3 — Sectional views in the longitudinal (Y-Z) and transverse (X-Z) planes and field components in the projected aperture.

part, maintains the characteristic amplitude distribution of the TE_{10} mode as it proceeds along the horn; nevertheless, it is a spherical wave and undergoes inverse distance attenuation up to the point where it is rendered equiphase by the paraboloidal reflector. Thus, over the surface of the projected aperture, s in Fig. 3(a), the field has an unsymmetrical amplitude taper in the direction of the horn axis due to inverse distance attenuation in addition to the symmetrical characteristic of the TE_{10} mode.

In Fig. 3(b), two sets of vectors, t and l, representing transverse and longitudinal polarization in the projected aperture, are shown. On the bisector of the aperture, t is parallel to the x-axis and l to the y-axis; however, at points removed from the bisector, t and l preserve the polarization established in the pyramidal horn, and therefore are inclined with respect to the principal axes. At these points, t and l are broken down into components a, b and c, d respectively, as indicated in Fig. 3(b); note that there is asymmetry about the bisector in the cross components b and d.

The aperture field being known, one can calculate the field at a large distance R in the region near the axis of the beam to good approximation by

$$E = \frac{j}{\lambda R} \int_s E_i \, e^{-j\beta(y \sin \theta_l + x \sin \theta_t)} \, ds, \tag{1}$$

where E_i represents any one of the components a, b, c, or d, and θ_l and θ_t are angles in the principal plane, which either contains or is transverse to the axis of the pyramidal horn. The longitudinal plane contains the horn and beam axes; the transverse plane contains the beam axis and is normal to the axis of the horn. Thus, in Fig. 3, θ_l lies in the yz plane and θ_t in the xz plane. Both the principal and cross-polarized radiation patterns* may be computed using (1), provided the appropriate aperture field component E_i is chosen. The computed patterns are shown in Figs. 4, 5, and 6 as dashed curves†; the experimental data are shown as solid lines and will be discussed later. The two cross-polarization patterns in the longitudinal plane are zero for all angles since the aperture field components b and d are antisymmetrical with respect to that plane.

The radiation patterns for circular polarization may be calculated by combining the appropriate principal and cross-polarized components of the far field. An example of the method is given in Appendix B. The

* Details are given in Appendix A.

† The computations were made for points separated 0.25° in θ; thus, although the dashed curves extend to the −50 db level, they do not represent the depths of the nulls for the case of longitudinal plane patterns, but rather only their positions.

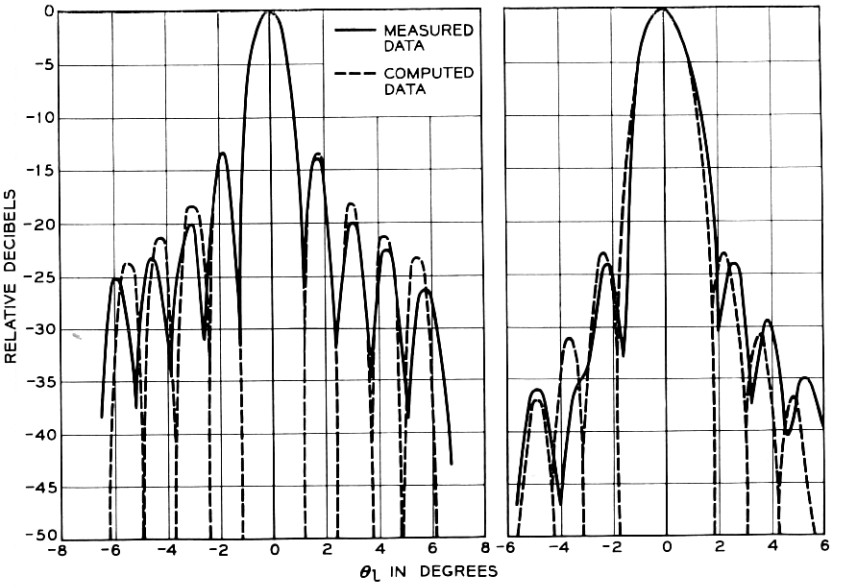

Fig. 4 — Principal radiation patterns in the longitudinal plane (2390 mc).

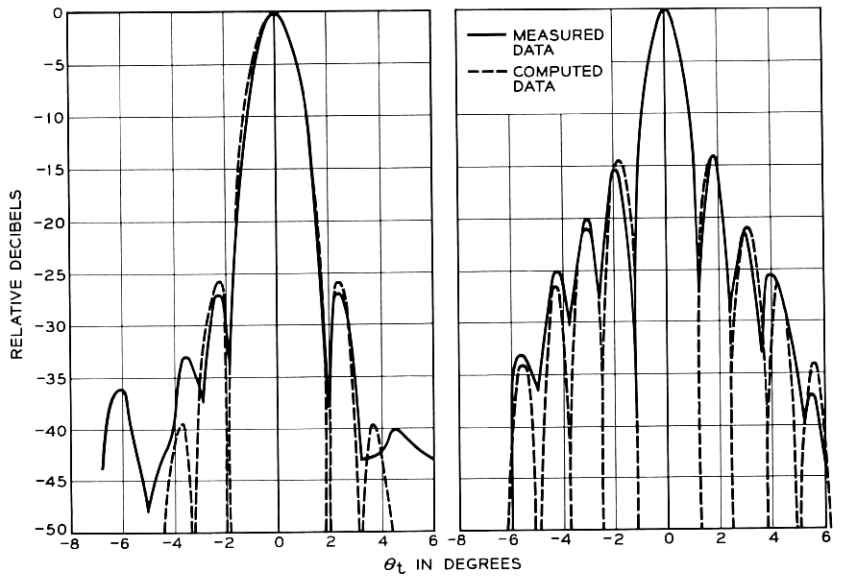

Fig. 5 — Principal radiation patterns in the transverse plane (2390 mc).

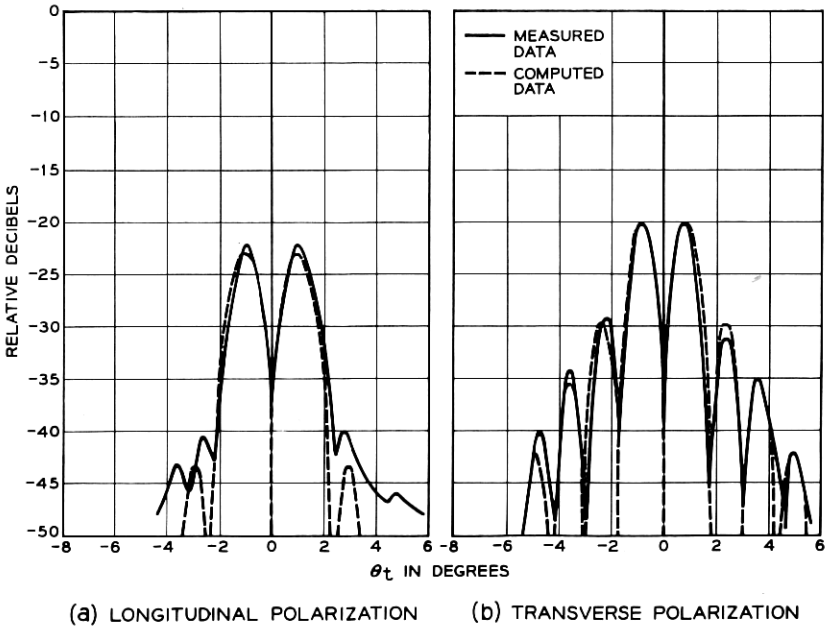

Fig. 6 — Cross-polarized radiation patterns in the transverse plane (2390 mc).

dashed lines of Figs. 7(a) and 8(a) show calculated radiation patterns where the antenna receives the desired (transmitted) sense of circular polarization, and Figs. 7(b) and 8(b) show the undesired sense. Note especially Figs. 8(a) and (b) for the transverse plane, in which the patterns are unsymmetrical with respect to the $\theta_t = 0$ axis; in Fig. 8(a), the maximum of the main beam is at $\theta_t = -0.1°$. This effect is more clearly demonstrated by assuming that the antenna receives both clockwise and counter-clockwise senses simultaneously, as would be the case for a linearly polarized incident wave; the beam, for one sense, shifts to $\theta_t = +0.1°$ and for the other to $\theta_t = -0.1°$; this effect is shown in Fig. 9. The slight tilting of the beam in circular polarization is a consequence of asymmetry in the phase of the cross-polarized components of the far field.

Unfortunately, all the energy which proceeds along the horn does not illuminate the paraboloidal reflecting surface; some of it is diffracted at the edge of the horn aperture. As indicated by the dashed line in Fig. 3(a), the wave is again diffracted by the edge of the reflector and produces perturbations in the far-field pattern. The lobes thus produced are referred to as spillover lobes; in Appendix D a method of calculating

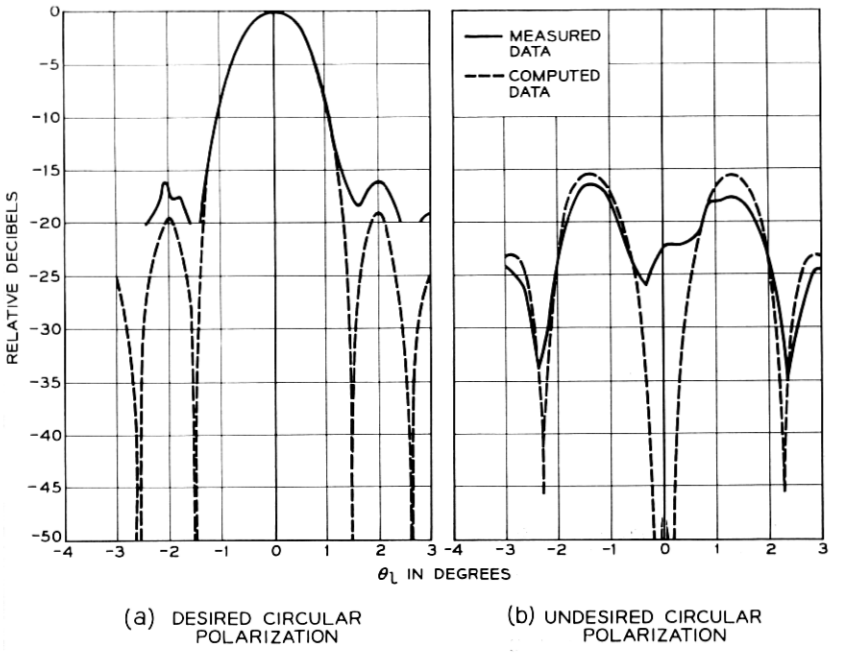

Fig. 7 — Circularly polarized radiation pattern in the longitudinal plane (2390 mc).

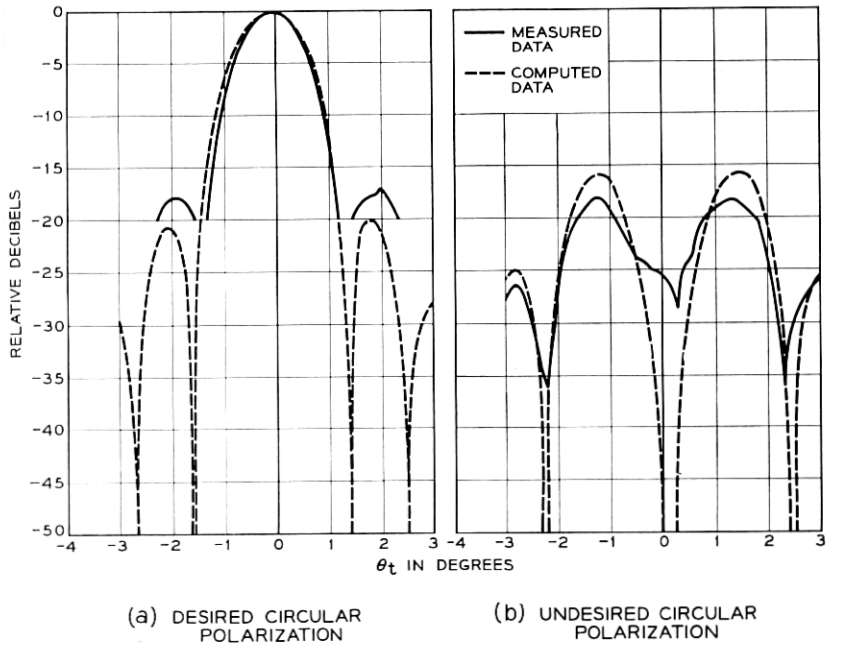

Fig. 8 — Circularly polarized radiation patterns in the transverse plane (2390 mc).

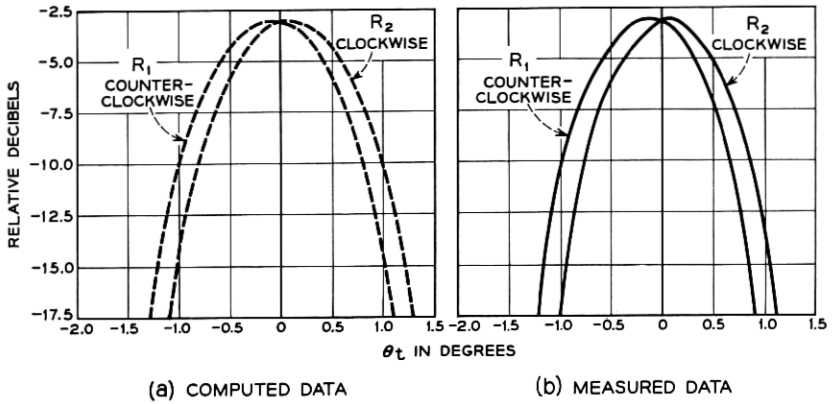

Fig. 9 — Circularly polarized radiation patterns in the transverse plane, showing dependence of beam displacement on sense of polarization.

them is discussed. The points in Fig. 10 show the spillover effect calculated for longitudinal polarization in the longitudinal plane. The maximum spillover energy is at an angle $\theta \simeq 70°$; as indicated in the insert in Fig. 11, this differs by 7° from the direction determined by the flare angle of the horn, namely, 77°. For transverse polarization, the spillover effect is much reduced because of the cosine distribution in the z direction in the horn for that polarization.

IV. TECHNIQUE OF MEASUREMENTS

The important electrical properties of the antenna to be measured are its gain and radiation patterns at the frequency of interest, in this case 2390 mc. To make such measurements, it is necessary to provide a

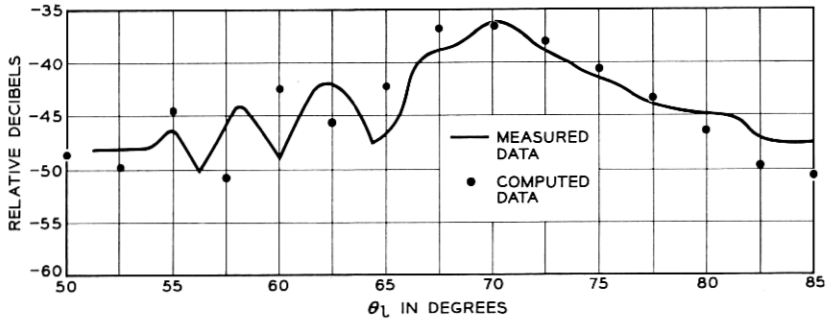

Fig. 10 — Calculated and measured spillover lobe; longitudinal plane, longitudinal polarization.

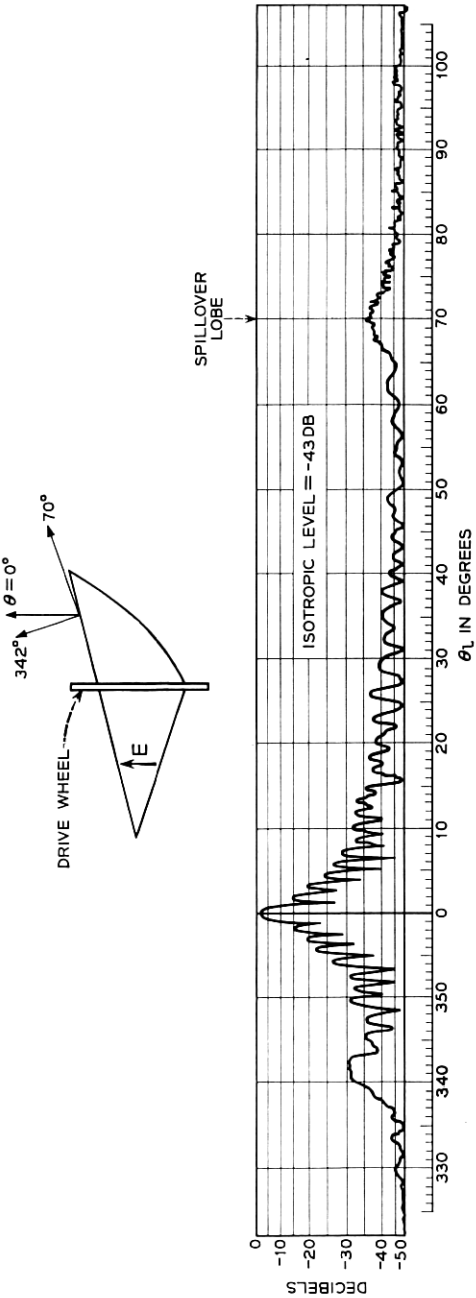

Fig. 11 — Extended radiation pattern; longitudinal plane, longitudinal polarization.

known incident field. In free space, ideally, the incident field would be uniform in amplitude and phase over the region occupied by the aperture of the antenna. In practice, this is accomplished by placing a source at a sufficient distance such that the wave incident at the antenna under test is essentially plane. The usual criterion is that the phase deviation over the aperture not exceed $\pi/8$. For the 20-foot aperture considered here, this criterion requires that a test transmitter operating at 2390 mc be at least one-third mile away; the distance used for these tests was about two miles. The antenna is not in free space, however, and environment such as trees and contours of the local terrain introduce reflections which distort the incident field. For these tests, nearby trees were removed and, both before and after the antenna was in place, the incident field was checked by exploring it with a probe consisting of a small horn. The horn was mounted on a motor-driven carriage that was drawn up and down a 55-foot vertical tower, the received output being continuously recorded. The tower was set at several horizontal positions so that the incident field over the area to be occupied by the antenna was mapped out. These height runs showed irregular variations in the incident field, but these did not exceed ± 1 db, and therefore were considered small enough to permit meaningful measurements. An analysis of the height runs indicated that, in addition to the direct space wave, a second wave, reflected from the intervening ground, was also present. The analysis fixed the reflection point at about midpath at an elevation corresponding to the tree-top level with an amplitude reflection coefficient of about 0.07.

V. GAIN MEASUREMENTS

The gain of the horn-reflector antenna was measured by comparing the strength of its received signal with that of a standard horn.* The latter was located in the plane of the aperture of the horn-reflector, but off to one side. The field at this particular location of the standard horn was equal to the average intensity of the field illuminating the horn reflector, as obtained from the height run data.

The measurement procedure consisted first of aiming the horn-reflector for optimum received signal strength and continuously recording the output. Because of scintillation of the signal, it was necessary to integrate for several seconds to obtain a dependable signal level. The coaxial line which fed the receiver was then shifted from the horn-reflector to the standard horn and the results recorded for a like period. A number of

* A pyramidal horn whose gain at 2390 mc, calculated from its physical dimensions, was 20.1 db.

such comparisons were made. The gain of the horn-reflector, referred to an isotropic radiator, was then obtained by adding the db difference between those two signal strengths to the db gain of the standard horn.

A double detection receiver was used in all the measurements. Signal-level differences were established by an attenuator in the intermediate frequency (65 mc) channel which was calibrated to an accuracy of ± 0.05 db. The gain was measured using both longitudinal and transverse polarizations and the results averaged:

Calculated gain of standard horn:	20.1 db,
Measured gain of horn-reflector over standard horn:	23.2 db,
Gain of horn-reflector:	43.3 db.

The rms scatter of the gain measurements was 0.16 db, due principally to scintillation of the signal.

The theoretical value for the horn-reflector gain is calculated by the method discussed in Appendix C. Due to the asymmetrical geometry of the aperture, the gain depends slightly on polarization, namely 43.43 db for longitudinal and 43.35 db for transverse. The average theoretical gain is therefore 43.39 db, which is 1.12 db below full area gain (44.51 db).

If we compare the measured and calculated values, the gain is 0.09 db less than expected.* Part of this discrepancy is due to the irregularities in the incident field discussed above in connection with the height run data. If one assumes that the variations in the phase of the incident field are random over the aperture, the deviation of the phase variation being derived from the 0.07 db reflection coefficient discussed above, one can estimate the decrease in received signal† due to this effect; this turns out to be 0.02 db, so that the discrepancy between calculated and measured values is reduced slightly. The remainder is most likely due to spillover.

VI. PATTERN MEASUREMENTS

Radiation patterns were obtained by continuously recording the receiver output as the horn-reflector was rotated at a constant speed.

There are several directional patterns of interest; these include the principal and cross-polarized patterns for the two linear polarizations in the two principal planes, and patterns in circular polarization for the

* In other words, the measured effective area is 1.2 db below actual area, or the measured efficiency, 76 per cent.

† For a small random fluctuation, the decrease in signal is $e^{-\delta^2}$ where δ is the standard deviation of the fluctuations in phase.[5]

two planes. As discussed in Section II, the two cross-polarized patterns in the longitudinal plane are expected to be zero, due to the odd symmetry of the cross-polarized components of the aperture field.

Detailed patterns for the principal polarizations in the region of the main beam are shown in Figs. 4 and 5 for longitudinal and transverse planes respectively. Measured data are shown by full lines and theoretical data by dashed lines. In general, the measurements agree very well with the calculated patterns except for some relatively small departures which are considered to be due to reflections from the environment and to scintillation. The salient factors obtained from the principal linear polarization patterns are shown in Table I.

The cross-polarization patterns in the transverse plane are shown in Fig. 6; here also the agreement between experiment and theory is considered to be good. The levels of cross-polarization in the longitudinal plane which are theoretically zero were lower than -30 db in the region near $\theta_l = 0$ and fell rapidly to less than -45 db for other angles.

The response of the antenna to circularly polarized waves is shown by the patterns of Figs. 7 through 9. In general, the agreement between measurement and theory is not as satisfactory as for the linear polarization patterns; this disagreement is believed due in part to lack of sufficient measuring range in the receivers used for the two circular senses. When both the transmitting test antenna and the horn-reflector were adjusted for the same sense of polarization, the first side lobes in both the longitudinal and transverse planes, as seen in Figs. 7(a) and 8(a), measured about 3 db higher than predicted by theory; the main beamwidths, however, agreed well with calculations. When the horn-reflector was adjusted to receive the sense opposite to that transmitted, the response on the first side lobes, as shown in Figs. 7(b) and 8(b), was about 2 db lower than predicted, while the response in the direction of the principal axis was about -27 db. The discrepancy between this value and that predicted by theory is believed due partly to depolarization by

TABLE I

Plane	Polarization	Beamwidths (3-db points)		Level of first minor lobes	
		Measured	Calculated	Measured	Calculated
transverse	longitudinal	1.35°	1.30°	−27.0db	−26.5 db
longitudinal	longitudinal	1.10°	1.10°	−13.5	−13.5
transverse	transverse	1.00°	1.00°	−14.5	−14.5
longitudinal	transverse	1.55°	1.55°	−24.0	−23.0

the ground and partly to imperfect circular polarization from the transmitter.*

A test was made in which the horn-reflector received simultaneously both senses of circular polarization which were generated by a wave from the test transmitter that was linearly polarized. The results appear in Fig. 9; the slight beam tilt, as evidenced by the displacement in opposite directions from $\theta = 0$ depending on the sense of polarization, agrees well with theoretical values. A similar displacement between the two senses was observed while receiving noise from the moon and sun.

Fig. 11 shows an extended radiation pattern measured in the longitudinal plane using longitudinal polarization. Let us refer to this region as the spillover sector; it is shown here in preference to any other sector because the level of the far-side lobes is of the order of the isotropic level rather than 10 to 30 db or so below isotropic, as is the case for the other sectors.[2,4] The most prominent spurious lobe is the so-called spillover lobe at an angle of 70° from the main beam. A more detailed plot of the spillover lobe is shown in Fig. 10, the points being values calculated in Appendix D. The agreement in level and shape of the measured and calculated curves is fairly good; however, the calculated data appear to be translated about two degrees toward smaller values of θ_l. Pattern measurements using transverse polarization showed much lower levels for the far lobes in the spillover sector.

Also apparent in Fig. 11 is a prominent lobe at angle 342°. This lobe is apparently associated with the 30-foot-diameter drive wheel, which, as may be seen in the insert in Fig. 11, tends to shadow the aperture in that direction. Diffraction over the rim of the wheel might be the cause of this spurious lobe.

VII. CONCLUDING REMARKS

The performance characteristics of a relatively large horn-reflector type of antenna, measured at a frequency of 2390 mc, agree satisfactorily with calculated performance. The measured radiation patterns are readily identified with those calculated to at least the third side lobes, the antenna gain being about one-tenth decibel less than expected. This good performance, in conjunction with the low-noise properties of this type of antenna, place it in a favorable position, not only for use in space communications, but also for use as a standard for absolute flux measurements in radio astronomy. Of some concern is a small amount of spill-

* The circular polarization was produced by a quarter-wave plate placed in front of the transmitting horn; the axial ratio, measured by rotating a 20-db horn antenna at the receiving site, was about 0.8 db.

over which degrades the performance in one sector of the radiation pattern; fortunately, in the above applications, the spillover sector is directed skyward and therefore the noise contribution is small in the microwave band.

Assistance in the assembly and adjustment of electrical components and in the measurement of the electrical properties of the antenna was given by R. A. Semplak, H. A. Gorenflo, and R. A. Desmond. Computation of the theoretical data was made by Mrs. C. L. Beattie.

APPENDIX A

Calculation of Patterns for Linear Polarization

The radiation patterns for linear polarization in the region of the main beam of the antenna are calculated using

$$E = \frac{j}{\lambda R} \int_s E_i \, e^{-j\beta(y \sin \theta_l + x \sin \theta_t)} \, ds, \tag{2}$$

where E_i is a component of the aperture field and x, y are coordinates in the projected aperture, S; R is the distance from the antenna to the

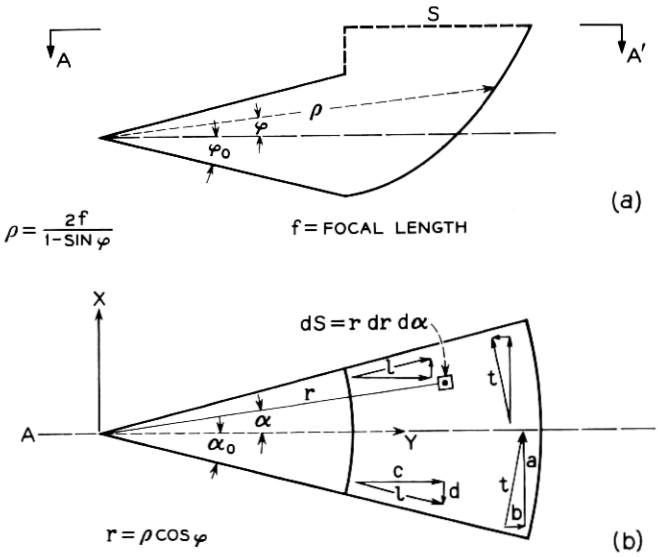

Fig. 12 — Coordinate system and projected aperture, S.

distant field point; θ_l and θ_t are angles in the principal planes; $\beta = 2\pi/\lambda$.

Since energy proceeds down the square horn in essentially a dominant waveguide mode, the field is constant along one coordinate and has a cosine distribution along the orthogonal coordinate. In addition, the field of the spherical wave decreases inversely with the distance ρ shown in Fig. 12(a), but, since the spherical phase front is corrected by the reflector, negligible attenuation occurs between the reflector and the projected aperture, S, in the plane AA'.

The total fields l and t, and the field components a, b, c, and d in the projected aperture, are shown in Fig. 12(b). Each of these can be expressed in terms of the symbols shown in the figure:

$$
\begin{aligned}
E_a &= E_0 \frac{\rho_0}{\rho} \cos \frac{\pi\varphi}{2\varphi_0} \cos \alpha, \\
E_b &= E_0 \frac{\rho_0}{\rho} \cos \frac{\pi\varphi}{2\varphi_0} \sin \alpha, \\
E_c &= E_0 \frac{\rho_0}{\rho} \cos \frac{\pi\alpha}{2\alpha_0} \cos \alpha, \\
E_d &= E_0 \frac{\rho_0}{\rho} \cos \frac{\pi\alpha}{2\alpha_0} \sin \alpha.
\end{aligned}
\tag{3}
$$

The field has been normalized to the value E_0 at $\rho = \rho_0 = 2f$ (where $\varphi = \alpha = 0$), φ_0 and α_0 being the flare angles of the horn. Equation (3), substituted for E_i in (2), results in the far-field equations. However, for comparison with experimental data, one must specify the principal plane of interest as well as the polarization; therefore let us designate the far fields in the following way:

Polarization of Antenna	*Plane of Measurement*	*Polarization of Far Field*	*Designation of Far Field*
longitudinal	longitudinal	longitudinal	E_1
transverse	longitudinal	transverse	E_2
longitudinal	transverse	longitudinal	E_3
transverse	transverse	transverse	E_4
longitudinal	longitudinal	transverse	E_5
transverse	longitudinal	longitudinal	E_6
longitudinal	transverse	transverse	E_7
transverse	transverse	longitudinal	E_8

These designations are related to (2) and (3) as follows:

$$\begin{bmatrix} E_1 \\ E_2 \\ E_5 \\ E_6 \end{bmatrix} = j\frac{4f^2}{\lambda R}\int_{-\alpha_0}^{\alpha_0} d\alpha \int_{-\varphi_0}^{\varphi_0} d\varphi \begin{bmatrix} E_c \\ E_a \\ E_d \\ E_b \end{bmatrix} \frac{\rho}{\rho_0}\frac{\cos\varphi}{1-\sin\varphi} e^{-j\beta\rho\cos\varphi\cos\alpha\sin\theta_t},$$

$$\begin{bmatrix} E_3 \\ E_4 \\ E_7 \\ E_8 \end{bmatrix} = j\frac{4f^2}{\lambda R}\int_{-\alpha_0}^{\alpha_0} d\alpha \int_{-\varphi_0}^{\varphi_0} d\varphi \begin{bmatrix} E_c \\ E_a \\ E_d \\ E_b \end{bmatrix} \frac{\rho}{\rho_0}\frac{\cos\varphi}{1-\sin\varphi} e^{-j\beta\rho\cos\varphi\sin\alpha\sin\theta_t}.$$

Integration shows that E_5 and E_6 are zero. The remainder are computed by numerical integration, with E_1, E_2, E_3, E_4, E_7, and E_8 corresponding to the patterns in Figs. 4(a), 4(b), 5(a), 5(b), 6(a), and 6(b) respectively.

APPENDIX B

Calculation of Patterns for Circular Polarization

The far-field patterns for circular polarization may now be calculated using the designations discussed in Appendix A. As an example, consider Fig. 13, in which the horn is assumed to be fed at the throat with a clockwise circularly polarized wave $-i_x - ji_z$, i_x and i_z being vectors

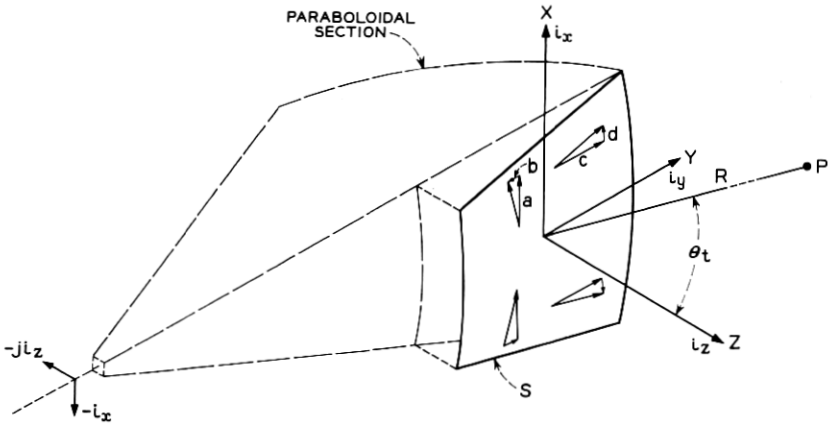

Fig. 13 — Aperture field components for calculation of circular polarization: distant point, P, is in the transverse plane.

in the x and z directions and $j = \sqrt{-1}$. Upon reflection by the paraboloidal section, this wave produces an aperture field

$$E_s = (i_x E_a - i_y E_b) + j(i_y E_c + i_x E_d), \tag{4}$$

i_y being in the y direction.* If we restrict the discussion to the transverse plane, E_a, E_b, E_c, and E_d are the aperture field components which produce the far fields E_4, E_8, E_3, and E_7 discussed above.† At a point P defined by a line R in the transverse plane making a small positive angle θ_t with respect to the z-axis, the field is

$$E_p = i_x E_4 - j i_y E_8 + j i_y E_3 - i_x E_7 . \tag{5}$$

In (5), account has been taken of the fact that the phase of the cross-polarized fields, E_7 and E_8, differs from that of the principal fields by 90°. Gathering together the x and y components, (5) becomes

$$E_p = i_x(E_4 - E_7) + j i_y(E_3 - E_8),$$

which can be broken down into two circularly polarized waves

$$E_{p_{\text{ccw}}} = \frac{i_x}{2}(E_3 + E_4 - E_7 - E_8) + j\frac{i_y}{2}(E_3 + E_4 - E_7 - E_8), \tag{6}$$

and

$$E_{p_{\text{cw}}} = \frac{i_x}{2}(E_3 - E_4 + E_7 - E_8) - j\frac{i_y}{2}(E_3 - E_4 + E_7 - E_8), \tag{7}$$

with (6) being the desired and (7) the undesired sense of rotation.

If the point P in Fig. 13 is below the z-axis such that θ_t is negative, the signs of the cross-polarized components E_7 and E_8 are reversed and the fields are

$$E_{p_{\text{ccw}}} = \frac{i_x}{2}(E_3 + E_4 + E_7 + E_8) + j\frac{i_y}{2}(E_3 + E_4 + E_7 + E_8) \tag{8}$$

and

$$E_{p_{\text{cw}}} = \frac{i_x}{2}(E_3 - E_4 - E_7 + E_8) - j\frac{i_y}{2}(E_3 - E_4 - E_7 + E_8). \tag{9}$$

Comparison of (6) with (8) and (7) with (9) shows that the radiation patterns in circular polarization will be somewhat unsymmetrical about the $\theta_t = 0$ axis.

* Note reversal in sense of polarization on reflection.

† Here, E_a, E_b, $\cdots$, E_4, E_8, $\cdots$ etc., are the amplitudes of the aperture and far fields.

In the longitudinal plane, since the cross-polarized fields are zero, the radiation patterns for circular polarization are symmetrical about $\theta_l = 0$.

APPENDIX C

Gain

The antenna gain may be calculated using

$$G = 4\pi R^2 \frac{F(0)}{P_s}, \tag{10}$$

where $F(0) = (1/\eta) \mid E(0)\mid^2$ is the density of power flow in the direction $\theta_l = \theta_l = 0$ as obtained from (2) by numerical integration ($\eta = 120\pi$); P_s, the total power radiated by the aperture is obtained by integration of either of the components l or t of Fig. 12. For example, since

$$E_l = E_0 \frac{\rho_0}{\rho} \cos \frac{\pi\varphi}{2\varphi_0}$$

and

$$ds = r\, dr\, d\theta = 4f^2 \frac{\cos\varphi}{(1 - \sin\phi)^2}\, d\varphi\, d\alpha,$$

$$P_s = \frac{E_0^2}{\eta} 4f^2 \int_{-\alpha_0}^{\alpha_0} d\alpha \int_{-\varphi_0}^{\varphi_0} d\varphi \cos^2 \frac{\pi\alpha}{2\alpha_0} \cos\varphi = \frac{E_0^2}{\eta} 8f^2\alpha_0 \sin\varphi_0 .$$

The efficiency of the antenna is given by A_e/S, where $A_e = \lambda^2 G/4\pi$ is the effective area and

$$S = \int_s r\, dr\, d\alpha = 16f^2\alpha_0 \frac{\sin\varphi_0}{\cos^2\varphi_0}$$

is the actual area of the projected aperture.

APPENDIX D

The Spillover Lobe

The spherical wave in the horn (shown in Fig. 14) is diffracted at edge A and part of the energy proceeds beyond the rim of the reflector, C. For the purpose of calculating the spillover lobe, the antenna configuration is idealized by replacing the curved reflector, shown dashed in Fig. 14, with a plane semi-infinite sheet, the edge of which is $c/2$ above the axis of the horn. The distant field of this horn-sheet combination can

then be calculated by use of Fourier transforms, as discussed by Woonton.[6] Restricting the discussion to the plane of Fig. 14, one obtains for the distant field at a point R, θ not too far removed from the axis of the horn:

$$E' = \left(\frac{j}{2\pi\lambda R}\right)^{\frac{1}{2}} E_0 e^{j(\pi-1)\gamma^2 b\lambda} \left\{\sqrt{\lambda l}\, e^{j\pi\gamma^2\lambda l}\,[C(v_2) - C(v_1) - jS(v_2) + jS(v_1)] - (1+j)\sqrt{\pi}\int_{-a/2}^{a/2} e^{-j\pi(h^2/\lambda l - 2\gamma h)}\,[C(v_0) - jS(v_0)]\,dh\right\}, \tag{11}$$

where E_0 is the field at the center of the horn aperture,

$$v_0 = \frac{1}{\sqrt{2b\lambda}}\,[c - 2(h - \gamma b\lambda)],$$

$$v_1 = \sqrt{\frac{2}{l\lambda}}\,[\gamma l\lambda - a/2],$$

$$v_2 = \sqrt{\frac{2}{l\lambda}}\,[\gamma l\lambda + a/2];$$

and $\gamma = -(1/\lambda)\sin(\pi/2 - \theta)$; a is the width of the horn aperture along the h coordinate; and b, c, l are the dimensions shown in Fig. 14, C and S being Fresnel integrals.

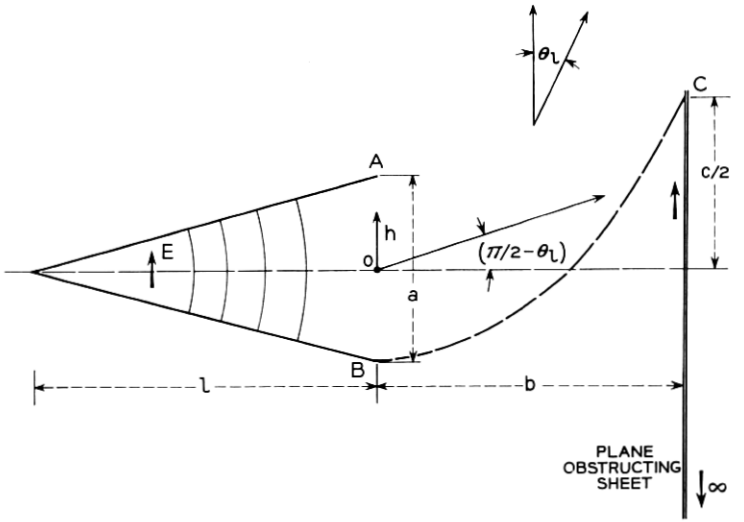

Fig. 14 — Two-dimensional geometry used for calculating the spillover lobe.

The two-dimensional solution, (11), predicts quite accurately the value of θ_l at which maximum spillover occurs, but it is in error in absolute value because in reality the diffracting edges A and C are of finite length and are curved. One can account approximately for the curvature of edge C by assuming that the diffraction effect in the plane of Fig. 14 and the effect in the plane AC, normal to the figure, are separable. In that case, (11) is multiplied by a factor

$$K = \frac{\int_{-d}^{d} e^{-j\pi(x^2/\lambda r)} \cos \frac{\pi x}{2d}\, dx}{\int_{-d}^{d} \cos \frac{\pi x}{2d}\, dx},$$

where x is the coordinate normal to the plane of Fig. 14 at C, $2d$ the extent of the edge along the x-axis, and r its radius of curvature.

The values plotted in Fig. 10 are KE'; K amounts to -10.5 db for the case under consideration.

REFERENCES

1. Friis, H. T., and Beck, A. C., U. S. Patent 2,236,393.
2. Friis, R. W., and May, A. S., A New Broad-Band Microwave Antenna System, A.I.E.E. Trans., Pt. I, **77**, 1958, p. 97.
3. Hogg, D. C., Problems in Low Noise Reception of Microwaves, I.R.E. Trans., Nat. Symp. on Space Electronics and Telemetry, 1960, p. 8–2.
4. DeGrasse, R. W., Hogg, D. C., Ohm, E. A., and Scovil, H. E. D., Ultra-Low-Noise Antenna and Receiver Combination for Satellite or Space Communication, Proc. Nat. Elect. Conf., **15**, 1959, p. 370.
5. Ruze, J., Nuovo Cimento, **9**, supp. 3, 1952, p. 364.
6. Woonton, G. A., The Effect of an Obstacle in the Fresnel Field on the Distant Field of a Linear Radiator, J. Appl. Phys., **21**, 1950, p. 577.